Dynamic and Static Determinations for Anisotropic Material Constants of Additive Manufacture in Nondestructive Testing

Yu-Hsi HUANG [1], Tai-Rong HUANG [1]
[1] National Taiwan University of Science and Technology, Taipei, Taiwan
Contact e-mail: yhhuang@mail.ntust.edu.tw

Abstract. This study used on the fused deposition modeling of 3D printer to process the specimens of three different directions. The specimens with different additive manufacture were measured their mechanical properties by static and the dynamic tests. The specimens of static test under the simply-supported beam boundary condition load the weight in the middle of specimens so that the Young's modulus were determined by measuring the deformation of strength. The specimens of dynamic test were achieved by the boundary condition of cantilever beam. Using a steel ball to strike the cantilever beam, the transient signal were obtained by two measured methods. Through the piezoelectric film bounded on the cantilever beam, the dynamic strain were determined by oscillator connecting with charge amplifier. Through the laser Doppler vibrometer (LDV) to measure the non-contact optical signals, the velocity were determined by the LDV built-in modulator. Using Fast Fourier Transform (FFT) to transfer the transient signals in time domain as frequency domain, the resonant frequency can be indicated by the maxima of frequency spectrums. Finally, the Young's modulus, Poisson's ratio, and shear modulus can be calculated according to the theory of Bernoulli-Euler beam. Finally, the orthotropic material constants of the additive manufacturing specimen can be built by those static and dynamic tests.

Introduction

Additive manufacturing, more popularly known a 3D printing, has been around since the 1980s; however, for decades patent issues slowed progress until the recent expiry of existing patents. Current manufacturing technologies include fused deposition modeling (FDM), stereolithography (SLA), and selective laser sintering (SLS). Unlike conventional manufacturing methods that remove unneeded material by turning or milling (subtractive manufacturing), 3D printing uses a layering technique (additive manufacturing), which greatly reduces the waste of materials, while enabling the completion of a workpiece in a single process. This in turn reduces labor and excessive energy consumption and makes it easy to create highly porous products. These advantages ensure that 3D printing will continue to develop well into the future. At present, these methods are widely applied in machinery, molding, and biomedicine. The ability to customize products is the main benefit, due to its ability to eliminate costly molding and an almost complete lack of restrictions with regard to the geometry of the products that can be produced. Most of the research on 3D printing has focused on the development of printing machines. Researchers have largely

disregarded the mechanical characteristics associated with the orientation of filaments. This study investigated the relationship between material strength and the geometric shape of structures, which is crucial in the customization of medical replacements for human tissue, such as teeth and bones.

In 2002, Li et al. [1] investigated the mechanics of anisotropic materials, making full use of the printing functions of FDM in an examination of the relationship between filament interval and density using measurements of Young's modulus, Poisson's ratio, and shear modulus in order to derive the Young's modulus lengthwise with the orientation of the filaments [0°/90°], [15°/-75°], [30°/-60°], and [45°/-45°]. In the same year, Ahn et al. [2] used FDM to print samples using acrylonitrile-butadiene-styrene (ABS) with orientations of [0°], [90°], [45°/-45°], and [0°/90°]. They then compared the tensile strength values with those obtained from molded specimens in accordance with ASTM D3039. In 2007, Lee et al. [3] employed FDM, SLA, and powder bed fusion in the fabrication of cylindrical specimens comprising ABS, resin reinforced with nanoparticles, or plaster, and measured the compressive strength according to ASTM D695. In 2014, Scholz et al. [4] investigated the tensile strength of composite resin materials containing no fibers, materials with fibers arranged in two directions, and materials with fibers arranged randomly. In the same year, Vallittu [5] implanted fibers into dentin in order to investigate the influence of fiber arrangement, continuous fibers, and short fibers on the strength of a unit volume of fibers. Shear and tensile strength tests confirmed that fibers of longer length provide greater tensile strength and Young's modulus, whereas the random arrangement of fibers had little effect. In this study, we employed a non-destructive testing method to derive nine material constants of specimens printed in a variety of build orientations in order to verify theoretical results using experiments and numerical calculation.

1. Basic Theory

1.1 Mechanics of Anisotropic Material

In the mechanics of anisotropic materials, Hooke's Law can be used to express the mechanical properties of anisotropic, orthotropic, transversely isotropic, and isotropic materials. Materials with strength or mechanical properties that vary with direction are anisotropic. The matrix relationship between stress and strain is as follows:

$$\begin{bmatrix} \sigma_{xx} \\ \sigma_{yy} \\ \sigma_{zz} \\ \tau_{yz} \\ \tau_{xz} \\ \tau_{xy} \end{bmatrix} = \begin{bmatrix} c_{11} & c_{12} & c_{13} & c_{14} & c_{15} & c_{16} \\ c_{12} & c_{22} & c_{23} & c_{24} & c_{25} & c_{26} \\ c_{13} & c_{23} & c_{33} & c_{34} & c_{35} & c_{36} \\ c_{14} & c_{24} & c_{34} & c_{44} & c_{45} & c_{46} \\ c_{15} & c_{25} & c_{35} & c_{45} & c_{55} & c_{56} \\ c_{16} & c_{26} & c_{36} & c_{46} & c_{56} & c_{66} \end{bmatrix} \begin{bmatrix} \varepsilon_{xx} \\ \varepsilon_{yy} \\ \varepsilon_{zz} \\ \gamma_{yz} \\ \gamma_{xz} \\ \gamma_{xy} \end{bmatrix} \quad (1)$$

where σ_{ij} and γ_{ij} denote normal stress and shear stress, respectively; ε_{ij} and τ_{ij} are normal stress and shear stress, in which i, j=1-3, and c_{ij} is the stiffness matrix. To simplify Eq. (1), we define the coordinate system conversions as follows:

$\sigma_{xx} \to \sigma_1$, $\sigma_{yy} \to \sigma_2$, $\sigma_{zz} \to \sigma_3$, $\tau_{yz} \to \tau_4$, $\tau_{xz} \to \tau_5$, $\tau_{xy} \to \tau_6$

If the material is also symmetrical with regard to the plane $y = 0$, then the conservation of strain energy means that $c_{45} = c_{16} = c_{26} = c_{36} = 0$; wherein Eq. (1) can be rewritten as

$$\begin{bmatrix}\sigma_1\\ \sigma_2\\ \sigma_3\\ \tau_4\\ \tau_5\\ \tau_6\end{bmatrix}=\begin{bmatrix}c_{11} & c_{12} & c_{13} & 0 & 0 & 0\\ c_{12} & c_{22} & c_{23} & 0 & 0 & 0\\ c_{13} & c_{23} & c_{33} & 0 & 0 & 0\\ 0 & 0 & 0 & c_{44} & 0 & 0\\ 0 & 0 & 0 & 0 & c_{55} & 0\\ 0 & 0 & 0 & 0 & 0 & c_{66}\end{bmatrix}\begin{bmatrix}\varepsilon_1\\ \varepsilon_2\\ \varepsilon_3\\ \gamma_4\\ \gamma_5\\ \gamma_6\end{bmatrix} \tag{2}$$

The engineering material constants inverse transform to Eq. (2) are

$$\begin{bmatrix}\varepsilon_1\\ \varepsilon_2\\ \varepsilon_3\\ \gamma_4\\ \gamma_5\\ \gamma_6\end{bmatrix}=\begin{bmatrix}\frac{1}{E_x} & -\frac{\nu_{yx}}{E_y} & -\frac{\nu_{zx}}{E_z} & 0 & 0 & 0\\ -\frac{\nu_{xy}}{E_x} & \frac{1}{E_y} & -\frac{\nu_{zy}}{E_z} & 0 & 0 & 0\\ -\frac{\nu_{xz}}{E_x} & -\frac{\nu_{yz}}{E_y} & \frac{1}{E_z} & 0 & 0 & 0\\ 0 & 0 & 0 & \frac{1}{G_{yz}} & 0 & 0\\ 0 & 0 & 0 & 0 & \frac{1}{G_{zx}} & 0\\ 0 & 0 & 0 & 0 & 0 & \frac{1}{G_{xy}}\end{bmatrix}\begin{bmatrix}\sigma_1\\ \sigma_2\\ \sigma_3\\ \tau_4\\ \tau_5\\ \tau_6\end{bmatrix} \tag{3}$$

where $\frac{\nu_{yz}}{E_y}=\frac{\nu_{zy}}{E_z}$, $\frac{\nu_{zx}}{E_z}=\frac{\nu_{xz}}{E_x}$, and $\frac{\nu_{xy}}{E_x}=\frac{\nu_{yx}}{E_y}$.

1.2 Theory underlying Dynamic Testing

1.2.1 Transverse & Lateral Bending Mode

According to the Euler-Bernoulli beam theory, deformation generated by shear forces is negligible, which means that the plane perpendicular to the neutral axis remains flat and perpendicular to the neutral axis, even when the cantilever beam bends and/or deforms due to the application of an external force. Thus, the bending moment and curvature of the cantilever beam can be expressed as

$$\frac{\partial^2}{\partial x^2}\left(EI\frac{\partial^2 y}{\partial x^2}\right)+\rho A\frac{\partial^2 y}{\partial t^2}=q(x,t) \tag{1}$$

Let $y(x,t)=Y(x)T(t)$ in the absence of the uniformly distributed load (q =0) and using the separation of variables, by substituting $y(x,t)=Y(x)T(t)$ into Eq. (9), we obtain

$$\frac{d^4Y(x)}{dx^4}-\beta^4Y(x)=0 \tag{2}$$

where

$$\beta^4=\frac{\omega^2}{a^2}=\frac{\rho A\omega^2}{EI} \tag{3}$$

Based on Eq. (2), we can assume that the general solution for displacement is

$$Y(x) = D_1(\cos\beta x + \cosh\beta x) + D_2(\cos\beta x - \cosh\beta x) + D_3(\sin\beta x + \sinh\beta x) + D_4(\sin\beta x - \sinh\beta x) \quad (4)$$

where D_1, D_2, D_3, and D_4 are the four coefficients to be determined based on the boundary conditions of the cantilever beam,

$$Y(0) = Y'(0) = Y''(\ell) = Y'''(\ell) = 0 \quad (5)$$

Boundary condition (5) can be substituted into Eq.（11), thereby giving $D_1 = D_2 = 0$ and the characteristic equation

$$\cos\beta\ell\cosh\beta\ell = -1 \quad (6)$$

to which the first six solutions are

$\beta_1\ell = 1.875$ $\beta_2\ell = 4.694$ $\beta_3\ell = 7.855$ $\beta_4\ell = 10.996$ $\beta_5\ell = 14.137$ $\beta_6\ell = 17.279$

When the actual dimensions of the cantilever beam are substituted into Eq. (3), we can derive the Young's modulus and natural frequency.

The vibration characteristics of the cantilever beam's lateral modes can be obtained by switching width b and height h in the moment of inertia.

1.2.2 Torsional mode

Similar with bending mode, the equation of torsional equilibrium is

$$\frac{\partial^2\theta}{\partial x^2} = \frac{1}{c_S^2}\frac{\partial^2\theta}{\partial t^2} \quad (7)$$

where

$$c_S = \sqrt{\frac{C_T}{\rho J}} = \frac{2h}{b}\sqrt{\frac{G}{\rho}} \quad (8)$$

Based on the torsional boundary condition of the cantilever beam, the natural frequency of the torsional mode is

$$f_n = \frac{w_n}{2\pi} = \frac{(2n-1)}{2l}\frac{h}{b}\sqrt{\frac{G}{\rho}},\ n = 1,2,3,... \quad (9)$$

Substituting the actual dimensions of the cantilever beam into Eq. (9), we can obtain the natural frequency of the torsional mode as well as the shear modulus at said natural frequency.

1.3 Theory underlying Static Testing

Euler-Bernoulli beam theory stipulates that the deformation generated by shear forces is negligible; i.e., the plane perpendicular to the neutral axis remains flat and perpendicular to the neutral axis even when the cantilever beam bends and/or deforms under the application of an external force. In the static test in this study, we employed the deflection formula of a simply-supported beam in conjunction with the moment area method in the derivation process [18]. The shear force and bending moment are shown in Fig. 1.

Based on the first moment area theorem,

$$\theta_B = \theta_A + \frac{1}{2}(\frac{L}{2})(\frac{FL}{4EI}) \quad (19)$$

Due to the symmetrical characteristics of the simply-supported beam, and based on the second moment area theorem,

we can derive the following:

$$\delta_B = \frac{L}{2}\theta_A + (\frac{FL^2}{16EI})(\frac{1}{3}\times\frac{L}{2}) = -\frac{FL^3}{48EI} \quad (20)$$

Then, by substituting into Eq. (20) the measured deformation and displacement, the magnitude of the load, and the dimensions of the simply-supported beam, we can obtain the Young's modulus.

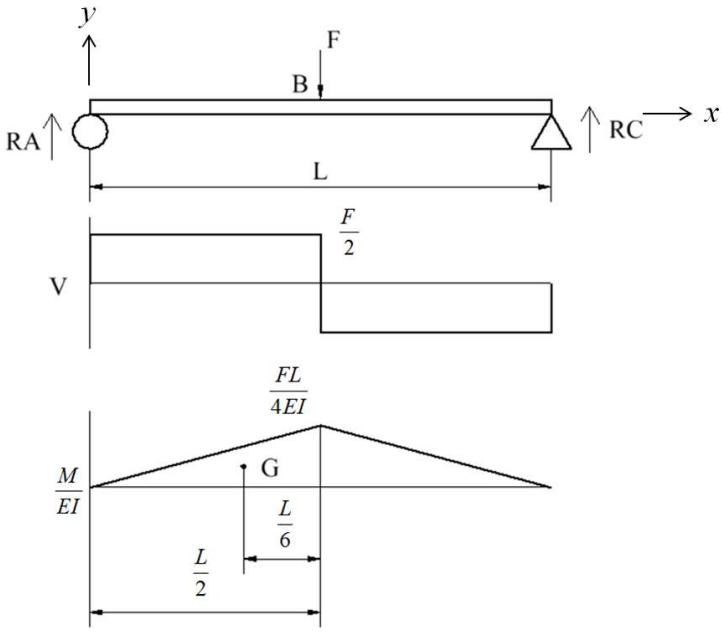

Fig. 1 Static testing setup to measure material constants of simply-supported beam

2. Experiment Setup

FDM is an additive manufacturing method in which material is heated until melted. Following the deposition of the material, the temperature drops below the melting point and the material automatically solidifies. By laying down material in layers from the bottom to the top, the product is gradually formed. FDM equipment and the materials used in FDM fabrication are simple and inexpensive. The FDM 3D printer used in this study, with a maximum printing range of 200 mm × 200 mm × 150 mm, with 150 mm being the z direction. Polymer materials such as ABS and PLA are generally used in FDM, and ABS was selected for this study.

The beam specimen with filaments oriented in the x direction (X-specimen) was 200 mm long in the x direction. It included 28 layers in the y-direction at intervals of 0.4 mm and 4 layers in the z-direction at intervals of 0.25 mm. Due to the effects of contraction, the actual dimensions of the finished specimen were 198 mm × 12.1 mm × 1.09 mm. The beam specimen with filaments oriented in the y direction (Y-specimen) was 198 mm × 12.25 mm × 1.18 mm. The beam specimen with filaments oriented in the z direction (Z-specimen) was 144.62 mm × 19.88 mm × 1.65 mm.

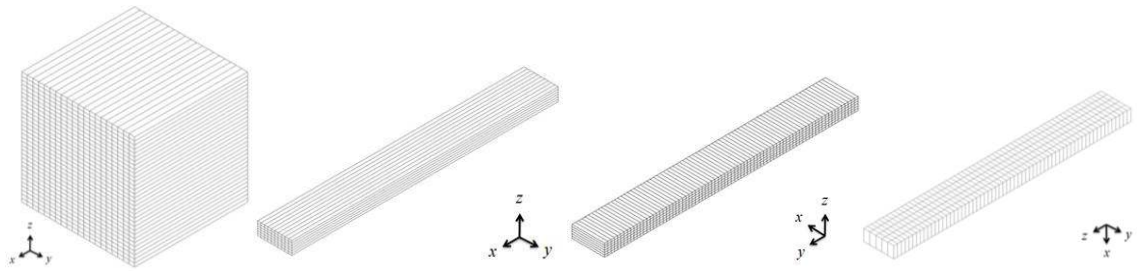

(a) (b) (c) (d)

Fig. 3 3D printed specimens: (a) diagram showing beam specimens with build orientation for filaments in the (b) x direction, (c) y direction, and (d) z direction

Transient signals in the time domain were generated by having a falling steel ball strike the beam. A PVDF piezoelectric film sensor and a non-contact LDV optical measurement system (Polytec PDV-100) were respectively used to obtain strain and velocity signals. FFT was then used to convert the transient signals into frequency responses. The frequencies associated with the first bending mode and torsional mode were substituted into Eqs. (3) and (9) to derive the material constants, which were then input into finite element calculations for the verification of resonant frequencies and vibration modes. Further verification was performed using the resonant frequencies obtained in the experiments. Figure 4(a) illustrates the setup used in the dynamic test. Figure 4(b) illustrates the locations of the two sensors on the cantilever beam and the two locations where the steel ball struck the beam to generate bending and torsional vibrations. The steel ball struck the beam twice at each of Impact Points A and B. Impact Point A was used to excite vibrations related to the bending mode of the cantilever plate, whereas Impact Point B was used to excite vibrations related to the torsional mode. Comparing the results of impacts at the two impact points made it possible to identify the resonant frequencies specific to bending and torsional modes.

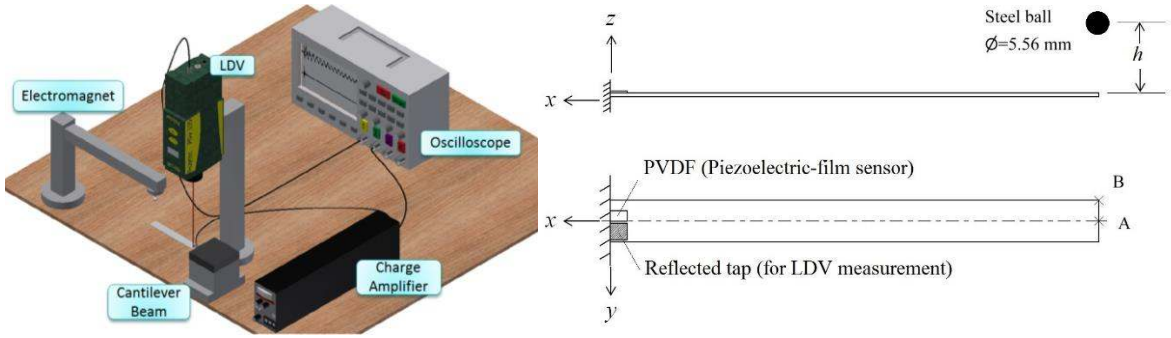

Fig. 4. (a) Setup used in dynamic test and (b)locations of sensors and steel ball impact points on the cantilever beams

3. Results

We first examine the results for the X-specimen with the cantilever beam fixed at one end. The clamped portion was not included in the calculations, which reduced the length of the beam to 150 mm. The reflective patch used to augment the dynamic signals from the PVDF sensor and LDV was placed at the fixed end, as shown in Fig. 4. The steel ball was dropped from a height of 29 mm and the test was conducted twice at Impact Points A and B, respectively. Figures 5 and 6 present the signals in the time domain and post-FFT signals in the frequency domain associated with a single impact from a falling steel ball at Impact Points A and B. The resonant frequencies are listed in Table 1.

Dynamic testing produced comprehensive material constants for the X-, Y, and Z-specimens fabricated at a flow rate of 70%. Eqs. (3) and (5) were used to construct the nine material constants required for the orthogonality matrix, as shown in Table 1. The nine material constants of the matrix were used as inputs for finite element analysis to calculate the resonant frequencies and vibration modes resulting from the anisotropic properties of the specimens. We then compared the FEM results with the theoretical results and experiment results averaged from the four impacts.

The Y-specimens and Z-specimens were subjected to the same dynamic and static tests. Table 2 compares the resulting material constants. In the static test, we were able to obtain the Young's modulus using the deflection formula; however, in the dynamic test, we were able to use the fundamental frequency to obtain the Young's modulus as well as the shear modulus, for use in deriving the Poisson’s ratio. For the Y-specimen, the Young's modulus obtained in dynamic testing was higher than that obtained in static testing.

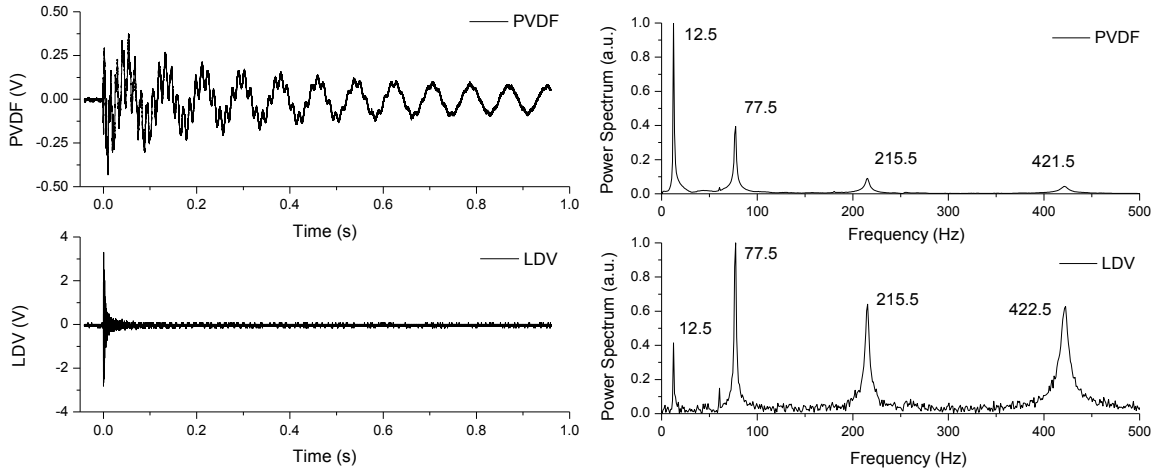

(a) (b)

Fig. 5 (a) Time-domain signals and (b) frequency-domain signals in X-specimens after being struck by steel ball at Impact Point A

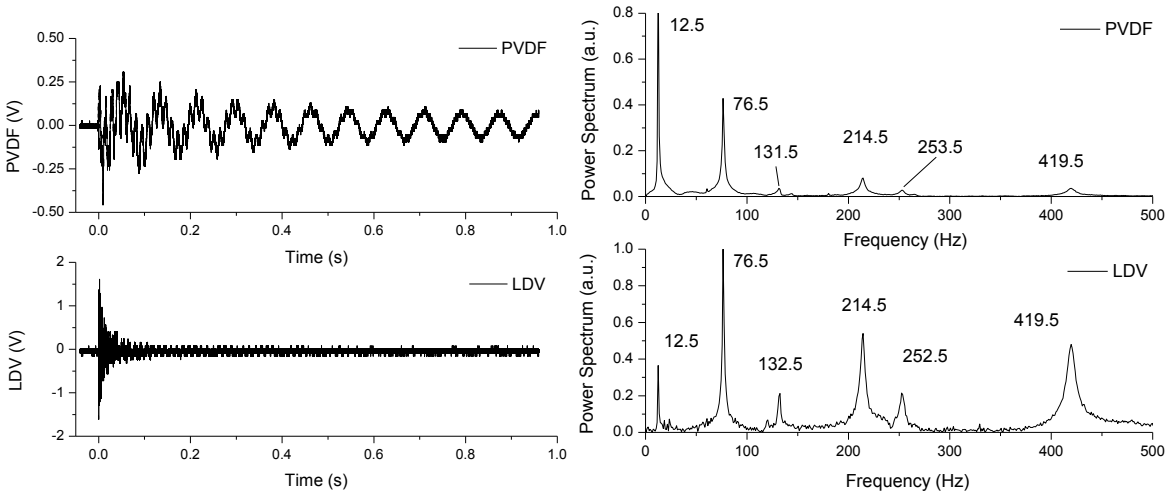

(a) (b)

Fig. 6 (a) Time-domain signals and (b) frequency-domain signals in X-specimens after being struck by steel ball at Impact Point B

Table 1 Material constants of orthogonality matrix (based on dynamic testing)

Elastic constants	$\times 10^6$ N/m^2	Compliance constants	$\times 10^{-11}$ m^2/N
c_{11}	2663.142	s_{11}	42.638
c_{12}	322.180	s_{12}	-3.888
c_{13}	552.284	s_{13}	-22.269
c_{22}	1549.678	s_{22}	70.314
c_{23}	346.294	s_{23}	-22.269
c_{33}	997.007	s_{33}	120.370
c_{44}	652.433	s_{44}	153.272
c_{55}	600.077	s_{55}	166.645
c_{66}	393.607	s_{66}	254.061

Table 4 Material constants from dynamic and static tests

	E_x (GPa)	G_{yz} (MPa)		E_y (GPa)	G_{xz} (MPa)
Dynamic test (x-70%)	2.34532	652.433	Dynamic test (y-70%)	1.42219	600.077
Static test (x-70%)	2.41123	--	Static test (y-70%)	1.17749	--

4. Conclusion

In this study, we conducted dynamic and static testing on 3D printed specimens with filaments oriented in various directions. The static test used the boundary conditions of a simply-supported beam with weights hung from the middle to observe deformation and displacement. The relationship between displacement and weight was used to calculate the Young's modulus. In the dynamic test, we used the boundary conditions of a cantilever beam fixed at one end. The impact from a falling steel ball was used to generate vibrations in the beam specimens, the transient signals of which were captured using an LDV and a PVDF sensor. The resonant frequencies were derived through the conversion of signals using FFT and then substituted into the Euler-Bernoulli beam equations to calculate the Young's modulus and shear modulus of the material. The results of the two experiments provide mutual verification regarding the accuracy of the material constants. If 3D printed products were indeed isotropic, then they would vary in their resistance to stress intensity under forces applied in different directions. Our results confirm that the products of additive manufacturing are indeed anisotropic. The influence of the direction in which force is applied could be therefore be derived using finite element analysis. Furthermore, our results suggest that printing filaments in the x direction will result in products with greater resistance to external force.

References

[1] Li, L., Sun, Q., Bellehumeur, C., and Gu, P., Composite Modeling and Analysis for Fabrication of FDM Prototypes with Locally Controlled Properties. Journal of Manufacturing Processes, 2002. 4(2): p. 129-141.
[2] Sung-Hoon Ahn, M.M., Dan Odell, Shad Roundy and Paul K. Wright, Anisotropic material properties of fused deposition modeling ABS. Rapid Prototyping Journal, 2002. 8(4): p. 248-257.
[3] Lee, C.S., Kim, S. G., Kim, H. J., and Ahn, S. H., Measurement of anisotropic compressive strength of rapid prototyping parts. Journal of Materials Processing Technology, 2007. 187–188(0): p. 627-630.
[4] Scholz, M.S., B.W. Drinkwater, and R.S. Trask, Ultrasonic assembly of anisotropic short fibre reinforced composites. Ultrasonics, 2014. 54(4): p. 1015-1019.
[5] Vallittu, P.K., High-aspect ratio fillers: Fiber-reinforced composites and their anisotropic properties. Dental Materials, 2015. 31(1): p. 1-7.
[6] Ma, C.C., Y.H. Huang, and S.Y. Pan, Investigation of the transient behavior of a cantilever beam using PVDF sensors. Sensors, 2012. 12(2): p. 2088-2117.